Numerical renormalization group calculations for the self-energy of the impurity Anderson model

1998 J. Phys.: Condens. Matter 10 8365

(http://iopscience.iop.org/0953-8984/10/37/021)

J. Phys.: Condens. Matter **10** (1998) 8365–8380. Printed in the UK PII: S0953-8984(98)93276-3

Numerical renormalization group calculations for the self-energy of the impurity Anderson model

R Bulla†, A C Hewson‡ and Th Pruschke§

† Max-Planck-Institut für Physik komplexer Systeme, Nöthnitzer Straße 38, 01187 Dresden, Germany

‡ Department of Mathematics, Imperial College, 180 Queen's Gate, London SW7 2BZ, UK

§ Institut für Theoretische Physik der Universität, 93040 Regensburg, Germany

Received 8 April 1998

Abstract. We present a new method for calculating directly the one-particle self-energy of an impurity Anderson model with Wilson's numerical renormalization group method by writing this quantity as the ratio of two correlation functions. This way of calculating $\Sigma(z)$ turns out to be considerably more reliable and accurate than that via the impurity Green's function alone. We give results for the self-energy for the case of a constant coupling between the impurity and the conduction band ($\mathrm{Im}\,\Delta(\omega + \mathrm{i}0^+) = \text{constant}$) and the effective $\Delta(z)$ arising in the dynamical mean-field theory of the Hubbard model. The implications of the problem of the metal–insulator transition in the Hubbard model are also discussed.

1. Introduction

The single-impurity Anderson model [1] is one of the most fundamental and probably the best understood model for strong electronic correlations. Since it was invented to describe the properties of magnetic impurities in non-magnetic metallic hosts 35 years ago, a variety of standard techniques have been applied to it and new methods have been developed to study its static and dynamic properties over basically the whole parameter space (for a review see e.g. [2]). Although a very clear picture of the physics of the single-impurity Anderson model has emerged from these calculations, a reliable method for calculating dynamic properties at very low temperatures and intermediate or large values of the Coulomb interaction was for a long time lacking.

For example, Bethe *ansatz* calculations [3], which are essentially exact, can only access static properties and the quantum Monte Carlo method [4], which can be viewed as another numerically exact technique, cannot reach very low temperatures and/or large values of the Coulomb parameter, although it does not suffer from a minus-sign problem here. In addition, the analytic continuation of the imaginary-time data to real frequencies is a numerically highly ill-conditioned problem.

Among the approximate treatments, the resolvent perturbation theory together with the so-called non-crossing approximation [5] turned out to be a simple and powerful technique for high and intermediate temperatures of the order of the Kondo scale but completely fails to reproduce the local Fermi-liquid properties as $T \to 0$. Last but not least, straightforward second-order perturbation theory in U [6] has been shown to work surprisingly well down to $T = 0$ but it is restricted to the symmetric case and not too large values of U.

0953-8984/98/378365+16$19.50

The numerical renormalization group (NRG) method, invented by Wilson for the Kondo problem [7] and later applied by Krishna-murthy *et al* to the impurity Anderson model [8], is usually acknowledged primarily in the context of universality and low-energy fixed-point behaviour of the Kondo or Anderson model. One of its most appealing features is that it can deal equally well with small, intermediate or large values of U and is not restricted to half-filling. During the last 15 years considerable progress has been made in extracting dynamical properties with this method, too, and it has been shown to give very accurate results also for e.g. dynamical one- and two-particle and also transport properties [9, 10]. The NRG method works best at $T = 0$, and various dynamical correlation functions can be calculated with an accuracy of a few per cent. Although less well defined for finite temperatures, its extension to $T > 0$ also shows very good agreement with exact results [10]. It is quite remarkable that no sum rules (Friedel sum rule, total spectral weight) need be used as input for these calculations. In contrast, they can serve as an independent check on the quality of the results.

More recent interest in reliable methods for solving the impurity Anderson model and calculating its dynamical properties has been motivated by the discovery that lattice models in the limit of infinite dimensions acquire a purely local one-particle self-energy [11]. This simplification eventually leads to a mapping of the lattice problem onto an effective-impurity Anderson model coupled to a medium to be determined self-consistently [12]. Note that in the general case the achieving of this self-consistency requires the knowledge of the one-particle self-energy. In view of the wide range of problems to which this so-called dynamical mean-field theory (DMFT; see e.g. [13]) can be applied, it seems surprising that there have been hardly any contributions using the NRG method. The only NRG calculation known to us is the work of Sakai *et al* [14] where the symmetric Hubbard model in the metallic regime was studied. In their paper, these authors point out some difficulties in the process of iterating the NRG results with the DMFT equations, which are largely related to the necessary broadening of the NRG spectra (see further below).

In this contribution we present a new method for calculating dynamical properties for the impurity Anderson model, namely by directly constructing the interaction contribution to the self-energy as the ratio of two correlation functions, $\Sigma_\sigma^U(z) = UF_\sigma(z)/G_\sigma(z)$, with $F_\sigma(z) = \langle\langle f_\sigma f_{\bar\sigma}^\dagger f_{\bar\sigma}, f_\sigma^\dagger\rangle\rangle_z$ and $G_\sigma(z) = \langle\langle f_\sigma, f_\sigma^\dagger\rangle\rangle_z$ (see section 2). Details of how to calculate the $F(z)$ are given in the appendix. In section 3 we discuss results for

(i) the standard case, where the coupling between impurity states and the metallic host, $\mathrm{Im}\,\Delta(\omega + \mathrm{i}0^+)$, is constant, and

(ii) the Hubbard model for $d = \infty$, where $\Delta(z)$ has to be determined self-consistently.

The Hubbard model is studied in the paramagnetic regime, at half-filling and $T = 0$. We discuss the properties of the self-energy and local density of states in both the metallic and insulating regimes and some preliminary results for the metal–insulator transition.

2. Calculation of the self-energy

2.1. The model and basic concepts

The impurity Anderson model is written in the form

$$H = \sum_\sigma \varepsilon_\mathrm{f} f_\sigma^\dagger f_\sigma + U f_\uparrow^\dagger f_\uparrow f_\downarrow^\dagger f_\downarrow + \sum_{k\sigma} \varepsilon_k c_{k\sigma}^\dagger c_{k\sigma} + \sum_{k\sigma} V_k \left(f_\sigma^\dagger c_{k\sigma} + c_{k\sigma}^\dagger f_\sigma \right). \tag{1}$$

In the model (1), $c_{k\sigma}^{(\dagger)}$ denote standard annihilation (creation) operators for band states with spin σ and energy ε_k, $f_\sigma^{(\dagger)}$ those for impurity states with spin σ and energy ε_f. The Coulomb interaction for two electrons at the impurity site is given by U and both subsystems are coupled via a hybridization V_k, which we allow to be k-dependent here.

Our final goal is to calculate the one-particle Green's function $G_\sigma(z) = \langle\langle f_\sigma, f_\sigma^\dagger\rangle\rangle_z$, which formally can be written as

$$G_\sigma(z) = \frac{1}{z - \varepsilon_f - \Sigma_\sigma(z)}. \tag{2}$$

While this formal introduction of the one-particle self-energy $\Sigma(z)$ is straightforward, the actual calculation of $G(z)$ or alternatively $\Sigma(z)$ is usually an extremely complicated problem. In order to express the self-energy $\Sigma(z)$ in terms of standard impurity correlation functions, we make use of the equation of motion

$$z\langle\langle A, B\rangle\rangle_z + \langle\langle \mathcal{L}A, B\rangle\rangle_z = \langle [A, B]_\eta\rangle \tag{3}$$

with $\mathcal{L}\,\cdot \equiv [H, \cdot]_-$ and $\eta = +$ if both A *and* B are fermionic operators, while $\eta = -$ otherwise. The correlation functions are defined as

$$\langle\langle A, B\rangle\rangle_z = \mathrm{i}\int_0^\infty \mathrm{e}^{\mathrm{i}zt}\langle [A(t), B]_\eta\rangle.$$

For $A = f_\sigma$ and $B = f_\sigma^\dagger$ we obtain the equation of motion for the f Green's function as

$$(z - \varepsilon_f)G_\sigma(z) - U\langle\langle f_\sigma f_{\bar\sigma}^\dagger f_{\bar\sigma}, f_\sigma^\dagger\rangle\rangle_z - \sum_k V_k\langle\langle c_{k\sigma}, f_\sigma^\dagger\rangle\rangle_z = 1. \tag{4}$$

The correlation function $\langle\langle c_{k\sigma}, f_\sigma^\dagger\rangle\rangle_z$ is related to $G_\sigma(z)$ via equation (3) with $A = c_{k\sigma}$ and $B = f_\sigma^\dagger$ through

$$(z - \varepsilon_k)\langle\langle c_{k\sigma}, f_\sigma^\dagger\rangle\rangle_z - V_k G_\sigma(z) = 0. \tag{5}$$

The U-term does not enter this equation as the Coulomb interaction only acts on the impurity states. Together with (5), equation (4) has the form

$$(z - \varepsilon_f)G_\sigma(z) - UF_\sigma(z) - \Delta(z)G_\sigma(z) = 1 \tag{6}$$

where we have defined

$$F_\sigma(z) = \langle\langle f_\sigma f_{\bar\sigma}^\dagger f_{\bar\sigma}, f_\sigma^\dagger\rangle\rangle_z \qquad \text{and} \qquad \Delta(z) = \sum_k V_k^2 \frac{1}{z - \varepsilon_k}.$$

The total self-energy $\Sigma_\sigma(z)$ for the single-impurity Anderson model is thus given by

$$\Sigma_\sigma(z) = \Delta(z) + \Sigma_\sigma^U(z) \tag{7}$$

where the non-trivial part due to the Coulomb correlations $\Sigma^U(z)$ is obtained from

$$\Sigma_\sigma^U(z) = U\frac{F_\sigma(z)}{G_\sigma(z)}. \tag{8}$$

For simplicity and since we are only interested in the paramagnetic situation for the time being, the spin index will be dropped in the following.

Alternatively, the interaction part of the self-energy can of course also be calculated directly from equation (2) using

$$\Sigma^U(z) = G_0(z)^{-1} - G(z)^{-1} \qquad \text{with } G_0(z) = \frac{1}{z - \varepsilon_f - \Delta(z)}. \tag{9}$$

At first glance, there seems to be no apparent reason to prefer the more complicated equation (8) over equation (9). In order to clarify the advantage of using equation (8) instead of equation (9) for the calculation of $\Sigma^U(z)$ with the NRG method we want to give a brief description of how the spectral densities for $G(z)$ and $F(z)$ are calculated with the NRG method.

2.2. Technical details

Within the NRG method, the impurity Anderson model equation (1) is mapped onto a semi-infinite chain (see [7, 8]) which is diagonalized iteratively starting from the uncoupled impurity. At each iteration, the number of states increases by a factor of 4 and, after a certain number of iterations, the basis kept for the next iteration has to be truncated. The important point of the method is that the coupling between consecutive elements of the chain decreases exponentially for increasing distance from the origin, so with increasing chain length at each iteration, basically only the lowest-lying states will be renormalized and such a truncation is meaningful. The spectral functions at each iteration are calculated from the corresponding matrix elements, which are in turn related to those of the previous iteration. This procedure is well established for the one-particle density of states $A(\omega) = -(1/\pi)\,\mathrm{Im}\,G(\omega + \mathrm{i}0^+)$ [9, 10] and can straightforwardly be extended to $B(\omega) = -(1/\pi)\,\mathrm{Im}\,F(\omega + \mathrm{i}0^+)$. For details we refer the reader to the appendix. Due to the truncation of states, the spectral function for the whole frequency range has to be built up from the data for all of the iterations.

The resulting spectral function is a set of δ-functions at frequencies ω_n with weights g_n which are broadened on a logarithmic scale as

$$g_n\delta(\omega - \omega_n) \longrightarrow g_n \frac{\mathrm{e}^{-b_n^2/4}}{b_n\omega_n\sqrt{\pi}} \exp\left[-\frac{(\ln\omega - \ln\omega_n)^2}{b_n^2}\right]. \tag{10}$$

This form of broadening was also used in [9] and [10] and is especially adapted to the exponential variation in energies peculiar to the NRG method. The width b_n is chosen as b independent of n, and we use values in the range $0.3 \leqslant b \leqslant 0.6$.

It is well known that with this scheme the NRG method already gives quite accurate results for $G(z)$ [9, 10]. However, one might anticipate some problems with the calculation of $\Sigma^U(z)$ using equation (9). The function $G_0(z)^{-1}$ is, of course, known exactly, since $\Delta(z)$ is a given quantity. Building the difference between an exactly known and a numerically determined function is usually very susceptible to numerical errors, especially in regions where the result becomes small. Since this is expected to happen close to the Fermi level, i.e. in the physically most relevant region, one is likely to run into problems there.

One naive attempt to reduce these kinds of inconsistency and numerical error when building the difference in equation (9) is to treat $G_0(z)^{-1}$ and $G(z)^{-1}$ on the same level—that is, to calculate $G_0(z)^{-1}$ via the NRG method as well by setting $U = 0$. However, since according to the theory of error propagation in sums or differences the absolute errors add, one must expect this procedure to be also ill-conditioned. If both $G_0(z)$ and $G(z)$ are known exactly, the difference $G_0(z)^{-1} - G(z)^{-1}$ always gives a negative imaginary part for the self-energy as there would be a pole in $G(z)^{-1}$ for every pole in $G_0(z)^{-1}$ at the same energy with equal or larger residue. This is no longer guaranteed as soon as both $G_0(z)$ and $G(z)$ are only known approximately, and one has to use rather large values of the broadening parameter b to avoid unphysical oscillations in $\Sigma^U(z)$. This broadening in turn leads to a strong suppression of the high-energy peaks because spectral weight is shifted from the centre of the peak to its tails (to the high-energy side due to equation (10)).

For the calculation of $\Sigma^U(z)$ via equation (8) on the other hand, we do not expect to face these kinds of problem to any great extent. Again, the two quantities are calculated on the same basis by broadening the NRG results with (10), i.e. with the same systematic error. This time, however, we *divide* them by each other, which means that only the *relative* errors will be propagated, leading to a numerically much more stable procedure.

Let us support this rather qualitative argument in favour of expressing the self-energy as

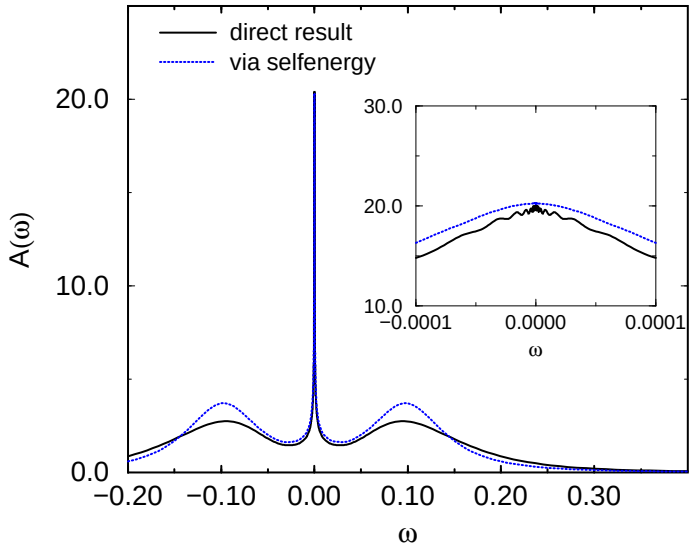

Figure 1. The impurity spectral function for $\varepsilon_f = -0.1$, $U = 0.2$, $T = 0$ and $-\mathrm{Im}\,\Delta(\omega+\mathrm{i}0^+) = 0.015$ in units of the conduction electron bandwidth. $\bar{A}(\omega)$ (solid line) is the result obtained directly from the NRG method and $A(\omega)$ (dashed line) is calculated via the self-energy equation (8). The inset shows the region around the Fermi level.

the ratio $UF(z)/G(z)$ by comparing the spectral function $\bar{A}(\omega)$ obtained directly from the NRG method (the solid line in figure 1) and the $A(\omega)$ calculated from equation (2) with the self-energy expressed as in equation (8) (the dashed line in figure 1). The spectral functions are defined as

$$A(\omega) = -\frac{1}{\pi}\,\mathrm{Im}\,G(\omega + \mathrm{i}0^+).$$

The parameters are $\varepsilon_f = -0.1D$, $U = 0.2D$ and $-\mathrm{Im}\,\Delta(\omega + \mathrm{i}0^+) = \Delta_0 = 0.015D$, where $2D$ is the conduction electron bandwidth. For convenience we use $D = 1$ as the energy scale and concentrate on the particle–hole-symmetric case of the Anderson model here. However, similar aspects also hold in the asymmetric case [15].

The differences between the two methods can be summarized as follows.

(i) We find for the total spectral weight

$$\int \mathrm{d}\omega\ \bar{A}(\omega) = \bar{w} = 0.93 \qquad \text{and} \qquad \int \mathrm{d}\omega\ A(\omega) = w = 0.9993.$$

The 7% deviation in $\bar{w}$ can in principle be reduced by improving the resolution of the NRG calculation (smaller deviations have been achieved e.g. in [9, 10]). This is, however, not necessary in our case, because the self-energy resulting from equation (8) is an analytic function and the sum rule $w = 1$ is then automatically fulfilled (apart from the very small numerical error).

(ii) The charge-fluctuation peaks near ε_f are much more pronounced in $A(\omega)$. That the high-energy features are usually underrated is a well-known problem in the calculation of dynamical properties with the NRG method. This problem is at least partially resolved in our new scheme, since the main contribution in this part of the spectrum comes instead from the hybridization part $\Delta(z)$, which is treated exactly.

(iii) The oscillations in $\bar{A}(\omega)$ near $\omega = 0$ are due to the fact that we use a very small broadening here and plot the spectral function on a very dense mesh (if one only plots the $\bar{A}(\omega)$ at frequencies $\omega_n \propto \Lambda^{-n}$, these oscillations are absent, as in [9, 10]). Nevertheless, these oscillations almost vanish in the final $A(\omega)$.

(iv) The impurity density at the Fermi level as deduced from the Friedel sum rule is

$$A(0) = -\frac{\sin^2(\delta)}{\pi \operatorname{Im} \Delta(\mathrm{i}0^+)} =: \frac{\sin^2(\delta)}{\pi \Delta_0}. \tag{11}$$

In the particle–hole-symmetric case, the scattering phase is $\delta = \pi/2$, so $A(0) \approx 21$ for the parameters used here. The results show a deviation from this value of about 7% in $\bar{A}(\omega)$ and 4% in $A(\omega)$.

Although the error in the Friedel sum rule is visibly reduced, the deviation is still a few per cent. Its origin will be discussed in the following.

2.3. Numerical aspects

It is important to understand the origin of the deviation of $A(0)$ (the Friedel sum rule) from its exact value, as this lies at the heart of the numerical procedure.

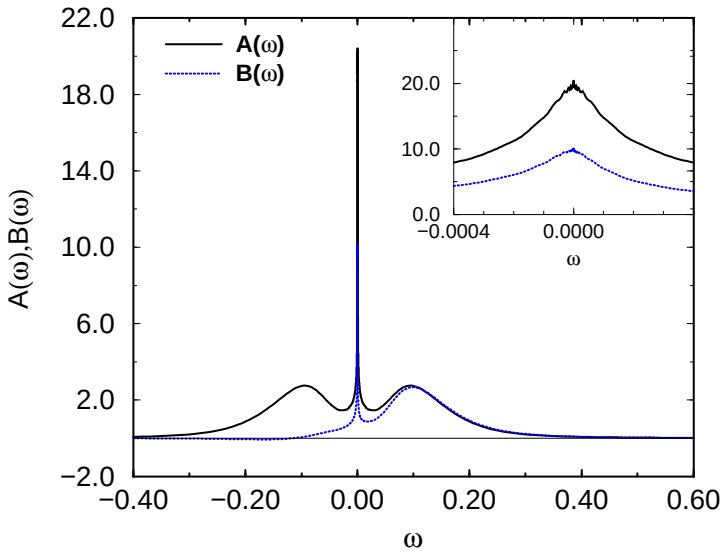

Figure 2. The spectral functions $A(\omega)$ (solid line) and $B(\omega)$ (dotted line) for the same parameters as in figure 1 (directly from the NRG method, not via the self-energy). The inset shows the region around the Fermi level.

Typical results for $A(\omega)$ and $B(\omega)$ as calculated with the NRG method are shown in figure 2. Both spectral functions $A(\omega)$ and $B(\omega)$ display a sharp resonance close to the Fermi energy. However, in contrast to $A(\omega)$, which is positive definite and perfectly symmetric about $\omega = 0$ due to the particle–hole symmetry, the function $B(\omega)$ is obviously not positive definite and appears to be extremely asymmetric.

As the next step, we must calculate the real parts, which are obtained via standard

Kramers–Kronig transformation. The self-energy is finally given, with equation (8), as

$$\mathrm{Re}\,\Sigma^U(\omega+\mathrm{i}0^+)+\mathrm{i}\,\mathrm{Im}\,\Sigma^U(\omega+\mathrm{i}0^+)=U\frac{\mathrm{Re}\,F(\omega+\mathrm{i}0^+)+\mathrm{i}\,\mathrm{Im}\,F(\omega+\mathrm{i}0^+)}{\mathrm{Re}\,G(\omega+\mathrm{i}0^+)+\mathrm{i}\,\mathrm{Im}\,G(\omega+\mathrm{i}0^+)}. \tag{12}$$

In the particle–hole symmetric case, $\mathrm{Re}\,G(\omega+\mathrm{i}0^+)$ necessarily vanishes at $\omega=0$; therefore,

$$\mathrm{Re}\,\Sigma^U(0^+)=U\frac{\mathrm{Im}\,F(\mathrm{i}0^+)}{\mathrm{Im}\,G(\mathrm{i}0^+)} \tag{13}$$

which of course has to give the Hartree term $U/2$, and

$$\mathrm{Im}\,\Sigma^U(\mathrm{i}0^+)=-U\frac{\mathrm{Re}\,F(\mathrm{i}0^+)}{\mathrm{Im}\,G(\mathrm{i}0^+)}. \tag{14}$$

In the case of the standard single-impurity Anderson model, we furthermore know that the Friedel sum rule $\mathrm{Im}\,\Sigma^U(\mathrm{i}0^+)=0$ has to be fulfilled, which implies that

$$\mathrm{Re}\,F(\mathrm{i}0^+)=-\int_{-\infty}^{\infty}\mathrm{d}\omega\;B(\omega)\,\mathcal{P}\frac{1}{\omega}=0 \tag{15}$$

where $\mathcal{P}(\cdots)$ denotes the principal value. Relation (15) is obviously not trivial as regards the unusual shape of $B(\omega)$. Indeed, it turns out that $\mathrm{Re}\,F(\mathrm{i}0^+)$ is numerically zero as long as the *full* spectrum of the Hamiltonian can be used. However, as soon as a truncation of states sets in, the calculated value for $\mathrm{Re}\,F(\mathrm{i}0^+)$ suddenly jumps to a finite value, eventually leading to a violation of the Friedel sum rule as observed e.g. in figure 1.

This observation suggests that high-energy states are also important to guarantee that $\mathrm{Re}\,F(\mathrm{i}0^+)=0$ and also that a slight violation of the Friedel sum rule is almost unavoidable in this method.

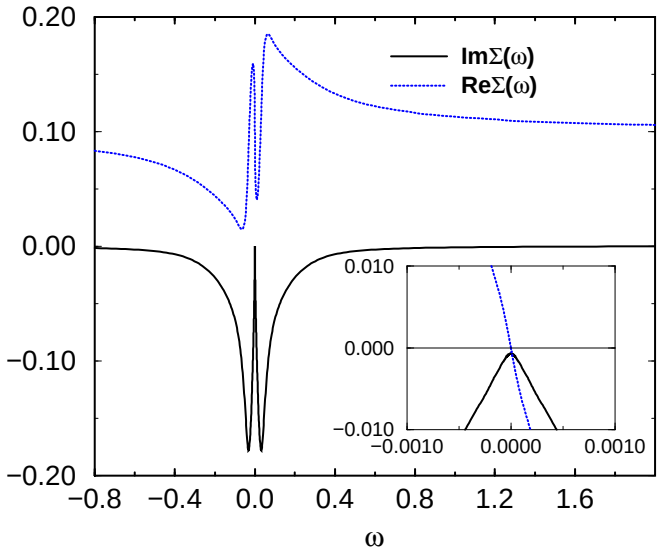

Figure 3. Real and imaginary parts of the self-energy for $\varepsilon_\mathrm{f}=-0.1$, $U=0.2$ and a constant $\Delta_0=0.015$. The inset shows the region around the Fermi level where the Hartree term was subtracted from the real part.

3. Results

3.1. The single-impurity Anderson model

As a simple example, let us discuss the standard case of a constant $\mathrm{Im}\,\Delta(\omega + \mathrm{i}0^+)$:

$$-\mathrm{Im}\,\Delta(\omega + \mathrm{i}0^+) = \begin{cases} \Delta_0 & |\omega| < 1 \\ 0 & |\omega| > 1. \end{cases} \tag{16}$$

The application of the NRG method to this model has been discussed very extensively in the literature [9, 10]. Thus the results presented here certainly give no new insight into the physics of this model. They are mainly intended to give the reader a feeling for the quality of our method.

Figure 3 shows the results for the real and imaginary part of $\Sigma^U(z)$ for $\varepsilon_\mathrm{f} = -0.1$, $U = 0.2$, $\Delta_0 = 0.015$ and $T = 0$. As a first important point we note that the real part of the self-energy has a constant contribution. If we calculate $\mathrm{Re}\,\Sigma^U(\omega) + \mathrm{Re}\,\Sigma^U(-\omega)$, we obtain the expected value $U/2$ to within numerical precision for all ω. This result also shows that, although $B(\omega)$ is asymmetric, the final result obeys the particle–hole symmetry to a high precision. In addition, the slope $\partial\,\mathrm{Re}\,\Sigma^U(\omega)/\partial\omega|_{\omega=0}$ is negative and large, corresponding to a high effective mass.

The imaginary part of $\Sigma^U(z)$ shows two pronounced peaks at $\omega \approx \pm 0.03$ and a steep decrease as $\omega \to 0$. In the vicinity of the Fermi level we find the Fermi-liquid property $\mathrm{Im}\,\Sigma^U(\omega + \mathrm{i}0^+) \propto \omega^2$ (see the inset of figure 3). However, as pointed out in the previous section, the Friedel sum rule $\mathrm{Im}\,\Sigma^U(\mathrm{i}0^+) = 0$ is not exactly fulfilled. The shift of $\mathrm{Im}\,\Sigma^U(\mathrm{i}0^+) \approx -0.0007$ corresponds to a 4% error in $A(0) = 1/(\pi\Delta_0)$.

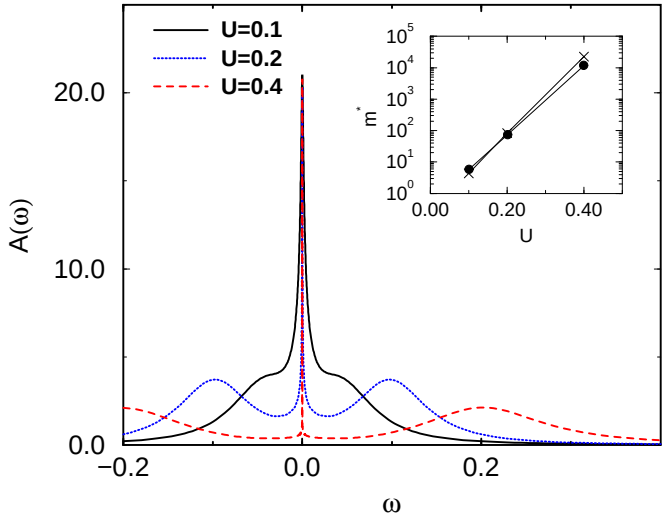

Figure 4. The spectral function for $\varepsilon_\mathrm{f} = -U/2$, $\Delta_0 = 0.015$ and various values of U. The inset shows the resulting effective mass m^* (filled circles) together with the expected behaviour $m^* \propto \sqrt{U}\exp(\pi U/(8\Delta_0))$ (crosses).

Figure 4, finally, shows the resulting spectral function for various values of U. As mentioned previously in section 2, we find pronounced charge-fluctuation peaks at $\pm U/2$ and the characteristic Abrikosov–Suhl resonance at the Fermi level. With increasing

U, this resonance becomes sharper. The corresponding energy scale expressed via the effective mass is shown in the inset to figure 4 together with the expected behaviour $m^* \propto \sqrt{U}\exp(\pi U/(8\Delta_0))$.

3.2. Application to the Hubbard model

The impurity Anderson model is not only useful to describe magnetic impurities in non-magnetic metals. It was shown only recently that in the limit of infinite spatial dimensions a lattice model (Hubbard model, periodic Anderson model etc) with local interactions can be mapped onto an effective single-impurity Anderson model. The quantity $\Delta(z)$, which in the single-impurity model describes the coupling to the metallic host, becomes in general an energy-dependent quantity here, which has a meaning similar to the Weiss field in the mean-field theory of the Heisenberg model. Since $\Delta(z)$ is a dynamical quantity which must be determined self-consistently as a functional of the one-particle self-energy [12–14], the name 'dynamical mean-field theory' (DMFT) has been coined.

This self-consistency makes it necessary to calculate the self-energy $\Sigma^U(z)$ as accurately as possible. Here we want to demonstrate that the NRG method together with the method of calculating $\Sigma^U(z)$ presented in the previous section is indeed a reliable and accurate method to do this job at $T = 0$.

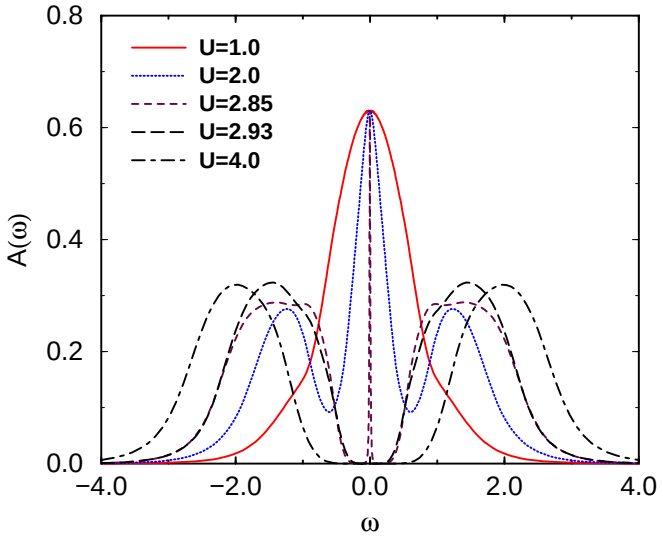

Figure 5. The local spectral function of the Hubbard model for various values of U. A quasiparticle peak develops for increasing values of U which vanishes at a critical value $U_c \approx 2.93$, signalling the metal–insulator transition.

The first step to take in order to apply the NRG method is the mapping of the impurity model onto a semi-infinite chain for the case of a non-constant $\mathrm{Im}\,\Delta(\omega + \mathrm{i}0^+)$, which we have already described in [16]. As the resulting $\mathrm{Im}\,\Delta(\omega + \mathrm{i}0^+)$ can develop very narrow structures at the Fermi level, we need a reliable numerical method to calculate ≈60–100 hopping matrix elements of the chain. This is done using arbitrary-precision Fortran routines. Apart from the difference in the hopping matrix elements, the calculation of $F(z)$, $G(z)$ and $\Sigma^U(z)$ follows the same procedure as in the flat-band case.

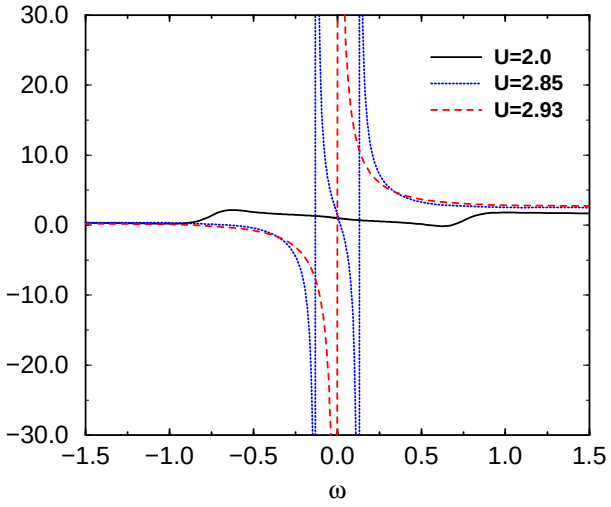

Figure 6. The real part of the self-energy for the Hubbard model (for the same parameters as in figure 5). The negative slope at $\omega = 0$ diverges at the metal–insulator transition. For $U \geqslant U_c$, the real part shows a $(1/\omega)$-divergence.

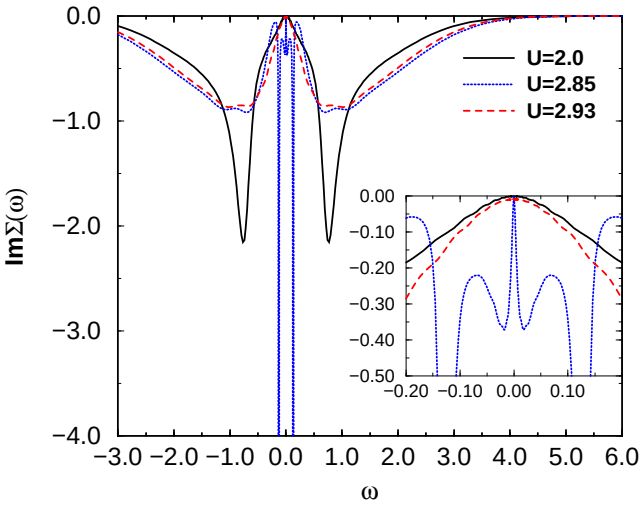

Figure 7. The imaginary part of the self-energy for the Hubbard model (for the same parameters as in figure 5). A δ-function develops for $U \to U_c$.

The simplest model for correlation effects in solids is the well-known Hubbard model [17]. This model is believed to have a rich phase diagram despite its comparatively simple form. DMFT studies at finite temperatures indeed revealed for example antiferromagnetic [18, 13] and ferromagnetic transitions [19, 20] and Mott–Hubbard metal–insulator transitions [13]. Nevertheless, there still remain lots of interesting open questions, especially about the properties of the model at extremely low temperatures both at and away from half-filling.

Here we study the Hubbard model at $T = 0$ for a semi-circular density of states $\rho_0(\varepsilon)$

corresponding to the Bethe lattice with infinite coordination number:

$$\rho_0(\varepsilon) = \frac{2}{\pi}\sqrt{1-\varepsilon^2} \tag{17}$$

($D = 1$) at particle–hole symmetry and in the paramagnetic regime. The resulting spectral functions for the paramagnetic Hubbard model for various values of U are collected together in figure 5. With increasing U, the one-particle spectrum develops the typical three-peak structure with a quasiparticle peak at $\omega = 0$ and the two Hubbard bands at $\pm U/2$. Above a certain value $U_c \approx 2.93$, the central peak vanishes and the system becomes insulating.

Figures 6 and 7 show the real and imaginary parts of the self-energy for the same parameters as in figure 5 ($U = 1$ and $U = 4$ are not shown). The Hartree term in the real part ($=U/2$) is subtracted. The negative slope at the Fermi level diverges as $U \to U_c$. For $U \geqslant 2.93$ (the insulating solution) the real part shows a $(1/\omega)$-divergence. The corresponding δ-peak in the imaginary part is not plotted in figure 7. This δ-peak in $\mathrm{Im}\,\Sigma^U(\omega)$ emerges from a two-peak structure in the metallic regime, with the positions of the two peaks approaching $\omega = 0$ for $U \to U_c$. The imaginary part shows the Fermi-liquid behaviour $\mathrm{Im}\,\Sigma^U(\omega) \propto \omega^2$ at low frequencies for $U < U_c$.

In order to give the reader an idea of the complex structures arising in lattice models, we show in figure 8 a comparison of the NRG flow diagram for the energy levels for the single-impurity Anderson model with flat $\mathrm{Im}\,\Delta(\omega)$ (figure 8(a)) and typical results for the Hubbard model in the paramagnetic metallic phase (figure 8(b)) and paramagnetic

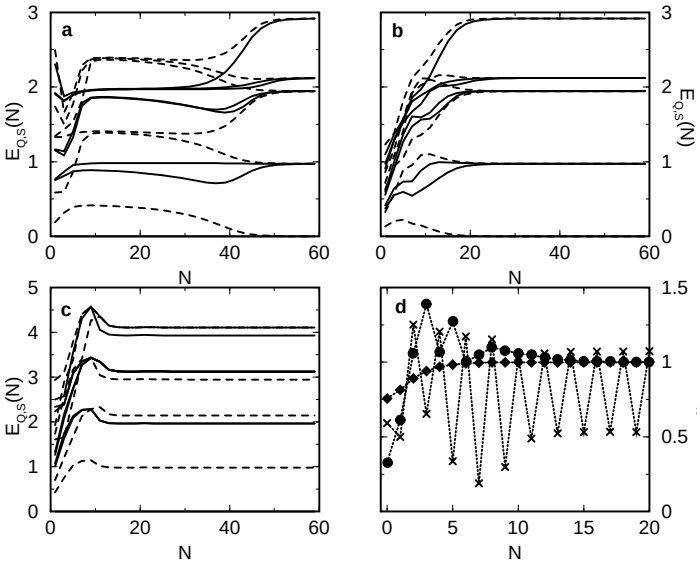

Figure 8. Flow diagrams for the lowest energy levels $E_{Q,S}$ as functions of the number of NRG iterations N. The solid lines correspond to quantum numbers $Q = 0, S = 1/2$ and the dashed lines to quantum numbers $Q = 1, S = 0$. (a) The flat-band case with $\varepsilon_f = -0.2$, $U = 0.4$ and a constant $\Delta_0 = 0.015$. For large N, the system flows to the Fermi-liquid fixed point, while in the intermediate regime ($N \approx 20$) it is near the so-called local moment fixed point. (b) The Hubbard model with $U = 2$ flows to the same Fermi-liquid fixed point as in the flat-band case. (c) The Hubbard model with $U = 4$ flows to the local moment fixed point corresponding to the insulating behaviour. (d) The hopping matrix elements t_N of the semi-infinite NRG chain for (a) (diamonds), (b) (circles) and (c) (crosses), respectively.

insulating phase (figure 8(c)). In contrast to the single-impurity case, the flow diagrams for the Hubbard model show a complicated crossover behaviour for high energies (low NRG iteration number) before they saturate into a fixed-point spectrum for large NRG iteration numbers, i.e. low energies. While these fixed-point spectra for the impurity model and the metallic solution of the Hubbard model (figures 8(a) and 8(b)) are identical, i.e. both correspond to a Fermi liquid, the fixed-point spectrum for the insulator (figure 8(c)) has a quite different structure (see e.g. the flow of the first excited state with $Q = 1, S = 0$ in figure 8(b) and figure 8(c); Q is defined as the particle number with respect to half-filling). In addition, the behaviour of the hopping matrix elements for the three cases is shown in figure 8(d) (diamonds, circles and crosses, respectively). Note the oscillatory behaviour in the latter case characteristic for a system with a (pseudo-) gap.

The data shown here are quite similar to those obtained by Georges *et al* [13] in that for U very close to U_c the quasiparticle peak seems to be isolated from the two Hubbard bands centred at $\omega = \pm U/2$. However, we always find very small but finite spectral weight in the region between the quasiparticle peak and the Hubbard bands. At the moment it is not clear whether this small spectral weight is a real physical effect or an artefact due to the broadening of the discrete δ-functions from the NRG procedure. This question is currently being investigated and a more detailed analysis of the metal–insulator transition at $T = 0$ will be presented in a subsequent publication.

For the time being we *define* the point where the transition from a metal to an insulator takes place by the divergence of the effective mass

$$m^* = 1 - \frac{\partial}{\partial\omega} \operatorname{Re} \Sigma^U(\omega)\Big|_{\omega=0} \tag{18}$$

of the quasi-particles. Note that this scenario completely neglects the possibility of a discontinuous transition for a $U < U_c$.

The behaviour of the effective mass as a function of U is shown in figure 9. m^* diverges at $U_c \approx 2.93$ and the critical behaviour close to U_c is consistent with a power law with an exponent of ≈ -2. Unfortunately, the data currently available do not allow a precise evaluation of this exponent. The value of U_c is significantly smaller than the

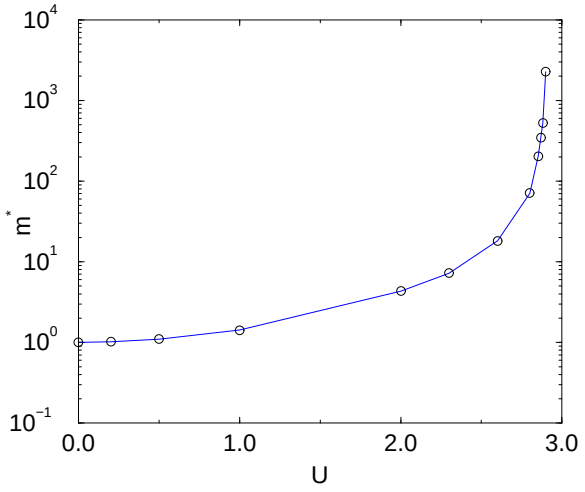

Figure 9. The U-dependence of the effective mass m^* for the Hubbard model. m^* diverges at $U_c \approx 2.93$ which defines the critical value of the metal–insulator transition.

value $U_{c,2} \approx 3.3$ found by Georges *et al* using the iterative perturbation theory, but in good agreement with the value $U_{c,2} = 2.92 \pm 0.05$ that they obtained from their self-consistent projective technique calculations [13]. It also agrees well with the value of $U_{c,2} = 3.02 \pm 0.05$. obtained in the NRG calculations of Shimizu and Sakai [14].

4. Summary

In this paper we have presented a new method for calculating the self-energy of the single-impurity Anderson model with the numerical renormalization group method. In contrast to the standard approach where one calculates the self-energy from the Green's function alone, we express $\Sigma^U(z)$ as a ratio of two correlation functions. The central aspect of this paper is that this method is much more accurate than the usual method.

The importance of this gain in accuracy goes beyond the mere improvement of the results for the single-impurity Anderson model. Our method now in addition allows one to apply the NRG method to various lattice models within the dynamical mean-field theory, where the self-energy of an effective impurity Anderson model has to be calculated self-consistently. As examples, we recapitulated typical results for the single-impurity Anderson model and presented results for the Hubbard model with a semi-circular density of states (corresponding to the Bethe lattice with infinite coordination number) at particle–hole symmetry and $T = 0$. For the latter we find a metal–insulator transition with a critical Coulomb interaction $U_c \approx 2.93$ and a diverging effective mass m^* as $U \nearrow U_c$.

A more detailed analysis of the metal–insulator transition, results for the Hubbard model away from particle–hole symmetry and the investigation of more complicated models (the periodic Anderson model, the three-band Hubbard model etc) will be discussed in forthcoming publications.

Acknowledgments

We wish to thank T Costi, J Keller and D Logan for a number of stimulating discussions. One of us (RB) was supported by a grant from the Deutsche Forschungsgemeinschaft, No Bu965-1/1. We are also grateful to the EPSRC for the support of a research grant (No GR/J85349).

Appendix A. The correlation function $F(z)$

Here we present some details of the calculation of $F(z)$ and discuss some of its properties.

The NRG method uses a discretized version of the Anderson model in a semi-infinite chain form (for details see [7, 8]). The resulting spectral functions will therefore be given as a set of discrete δ-peaks.

The spectral representation of $F(z)$ is

$$B(\omega) = \frac{1}{Z}\sum_{nm}\langle n|f_\downarrow f_\uparrow^\dagger f_\uparrow|m\rangle\langle m|f_\downarrow^\dagger|n\rangle\delta(\omega - (E_m - E_n))(\mathrm{e}^{-\beta E_n} + \mathrm{e}^{-\beta E_m}). \tag{A1}$$

The matrix elements $\langle n|f_\downarrow f_\uparrow^\dagger f_\uparrow|m\rangle$, $\langle m|f_\downarrow^\dagger|n\rangle$ and the energies E_n, E_m are calculated iteratively in the NRG method. The two operators

$$V_{1/2}^{1/2} = f_\downarrow f_\uparrow^\dagger f_\uparrow \qquad V_{-1/2}^{1/2} = -f_\uparrow f_\downarrow^\dagger f_\downarrow \tag{A2}$$

transform as

$$\begin{aligned}\left[s^{\pm}, V_q^{1/2}\right]_- &= \sqrt{\frac{3}{4} - q(q \pm 1)}\, V_{q\pm 1}^{1/2} \\ \left[s_z, V_q^{1/2}\right]_- &= q V_q^{1/2}\end{aligned} \tag{A3}$$

($q = \pm 1/2$), with the spin operators

$$\begin{aligned}s^+ &= f_\uparrow^\dagger f_\downarrow \qquad s^- = f_\downarrow^\dagger f_\uparrow \\ s_z &= \frac{1}{2}(f_\uparrow^\dagger f_\uparrow - f_\downarrow^\dagger f_\downarrow).\end{aligned} \tag{A4}$$

This allows us to use the Wigner–Eckart theorem:

$$\langle Q, S, S_z, w|\, V_q^{1/2}\, |Q', S', S_z', w'\rangle = \langle Q, S, w||V_q^{1/2}||Q', S', w'\rangle\langle S', S_z', \tfrac{1}{2}, q|S, S_z\rangle. \tag{A5}$$

The $\langle Q, S, w||V_q^{1/2}||Q', S', w'\rangle$ are reduced matrix elements and the $\langle S', S_z', \frac{1}{2}, q|S, S_z\rangle$ are Clebsch–Gordan coefficients. It is important to note that the operators $V_q^{1/2}$ transform in exactly the same way as the two operators

$$W_{1/2}^{1/2} = f_\uparrow^\dagger \qquad W_{-1/2}^{1/2} = f_\downarrow^\dagger. \tag{A6}$$

This has the consequence that all of the recursion formulae for the reduced matrix elements of $W_q^{1/2}$ can be used for the calculation of the reduced matrix elements of $V_q^{1/2}$. The only changes are in the particle numbers Q of the states involved and the initial values (see below).

The states $|n\rangle$ and $|m\rangle$ in equation (A1) are classified in terms of the charge Q (the total particle number relative to the half-filled case), the total spin S, the z-component of the total spin S_z and an additional label w:

$$\begin{aligned}|n\rangle &= |Q_n, S_n, S_{z,n}, w_n\rangle \\ |m\rangle &= |Q_m, S_m, S_{z,m}, w_m\rangle.\end{aligned} \tag{A7}$$

The sum over $S_{z,n}$ and $S_{z,m}$ in equation (A1) can be performed exactly and we find

$$\begin{aligned}B(\omega) = \frac{1}{Z} \sum_{\substack{Q,S,w_n \\ S_m = S\pm 1/2, w_m}} & \langle Q, S, w_n||V_{1/2}^{1/2}||Q+1, S_m, w_m\rangle \\ & \times \langle Q+1, S_m, w_m||f_\downarrow^\dagger||Q, S, w_n\rangle \delta(\omega - (E_m - E_g)) \\ & \times (\mathrm{e}^{-\beta E_n} + \mathrm{e}^{-\beta E_m}) \frac{1}{\sqrt{2}} \sqrt{2S+1} \begin{cases} \sqrt{S} & S_m = S - \frac{1}{2} \\ -\sqrt{S+1} & S_m = S + \frac{1}{2}. \end{cases}\end{aligned} \tag{A8}$$

We are only interested in the limit of zero temperature, where we have

$$\begin{aligned}B^+(\omega) = \frac{1}{Z} \sum_{S_m = S_g \pm 1/2} \sum_{w_m} & \langle Q_g, S_g, w_g||V_{1/2}^{1/2}||Q_g+1, S_m, w_m\rangle \\ & \times \langle Q_g+1, S_m, w_m||f_\downarrow^\dagger||Q_g, S_g, w_g\rangle \delta(\omega - (E_m - E_g)) \\ & \times \frac{1}{\sqrt{2}} \sqrt{2S_g+1} \begin{cases} \sqrt{S_g} & S_m = S_g - \frac{1}{2} \\ -\sqrt{S_g+1} & S_m = S_g + \frac{1}{2} \end{cases}\end{aligned} \tag{A9}$$

for positive frequencies and

$$B^-(\omega) = \frac{1}{Z}\sum_{S_n=S_g\pm 1/2}\sum_{w_n}\langle Q_g-1, S_n, w_n||V^{1/2}_{1/2}||Q_g, S_g, w_g\rangle \times \langle Q_g, S_g, w_g||f^\dagger_\downarrow||Q_g-1, S_n, w_n\rangle\delta(\omega-(E_g-E_n)) \times \frac{1}{\sqrt{2}}\sqrt{2S_g+1}\begin{cases}-\sqrt{S_g} & S_n = S_g-\frac{1}{2}\\ \sqrt{S_g+1} & S_n = S_g+\frac{1}{2}\end{cases} \tag{A10}$$

for negative frequencies. The ground-state is labelled by $|g\rangle = |Q_g, S_g, S_{z,g}, w_g\rangle$, the ground-state energy is E_g and the partition function Z reduces to the ground-state degeneracy.

To set up the iterative calculation of the reduced matrix elements

$$\langle Q_n, S_n, w_n||V^{1/2}_{1/2}||Q_m, S_m, w_m\rangle$$

we first of all need the initial values for the uncoupled impurity. The only non-zero matrix element is

$$\langle 0, \tfrac{1}{2}||V^{1/2}_{1/2}||1, 0\rangle = -1 \tag{A11}$$

in contrast to the two initial values

$$\begin{aligned}&\langle 0, \tfrac{1}{2}||f^\dagger_\downarrow||-1, 0\rangle = 1\\ &\langle 1, 0||f^\dagger_\downarrow||0, \tfrac{1}{2}\rangle = -\sqrt{2}.\end{aligned} \tag{A12}$$

Apart from the difference in the initial values and the fact that $Q_m = Q_n + 1$ for the $\langle\ ||V^{1/2}_{1/2}||\ \rangle$ matrix elements, the recursion relations for the two reduced matrix elements are identical and are given by

$${}_N\langle Q, S, w||V^{1/2}_{1/2}||Q', S', w'\rangle_N = \sum_{rr'}\sum_{pp'=1}^{4} U_{QS}(w, rp)U_{Q'S'}(w', r'p')\,{}_N\langle Q, S, r; p||V^{1/2}_{1/2}||Q', S', r'; p'\rangle_N \tag{A13}$$

with $p, p' \in \{1, 2, 3, 4\}$. The $U_{Q,S}$ are the unitary matrices which diagonalize the Hamiltonian matrix in the subspace with charge Q and spin S. The reduced matrix elements on the right-hand side of equation (A13) are given by

$${}_N\langle Q, S, r; 1||V^{1/2}_{1/2}||Q+1, S\pm\tfrac{1}{2}, r'; 1\rangle_N = {}_{N-1}\langle Q+1, S, r||V^{1/2}_{1/2}||Q+2, S\pm\tfrac{1}{2}, r'\rangle_{N-1}$$

$${}_N\langle Q, S, r; 2||V^{1/2}_{1/2}||Q+1, S+\tfrac{1}{2}, r'; 2\rangle_N = -\frac{2\sqrt{S^2+S}}{2S+1}\,{}_{N-1}\langle Q, S-\tfrac{1}{2}, r||V^{1/2}_{1/2}||Q+1, S, r'\rangle_{N-1}$$

$${}_N\langle Q, S, r; 2||V^{1/2}_{1/2}||Q+1, S-\tfrac{1}{2}, r'; 2\rangle_N = -{}_{N-1}\langle Q, S-\tfrac{1}{2}, r||V^{1/2}_{1/2}||Q+1, S-1, r'\rangle_{N-1}$$

$${}_N\langle Q, S, r; 3||V^{1/2}_{1/2}||Q+1, S+\tfrac{1}{2}, r'; 3\rangle_N = -{}_{N-1}\langle Q, S+\tfrac{1}{2}, r||V^{1/2}_{1/2}||Q+1, S+1, r'\rangle_{N-1}$$

$${}_N\langle Q, S, r; 3||V^{1/2}_{1/2}||Q+1, S-\tfrac{1}{2}, r'; 3\rangle_N = -\frac{2\sqrt{S^2+S}}{2S+1}\,{}_{N-1}\langle Q, S+\tfrac{1}{2}, r||V^{1/2}_{1/2}||Q+1, S, r'\rangle_{N-1}$$

$${}_N\langle Q, S, r; 2||V^{1/2}_{1/2}||Q+1, S-\tfrac{1}{2}, r'; 3\rangle_N$$

$$= -\frac{1}{2S+1}\,{}_{N-1}\langle Q, S-\tfrac{1}{2}, r||V^{1/2}_{1/2}||Q+1, S, r'\rangle_{N-1}$$

$${}_{N}\langle Q, S, r; 3||V^{1/2}_{1/2}||Q+1, S+\tfrac{1}{2}, r'; 2\rangle_{N}$$

$$= \frac{1}{2S+1}\,{}_{N-1}\langle Q, S+\tfrac{1}{2}, r||V^{1/2}_{1/2}||Q+1, S, r'\rangle_{N-1}$$

$${}_{N}\langle Q, S, r; 4||V^{1/2}_{1/2}||Q+1, S\pm\tfrac{1}{2}, r'; 4\rangle_{N} = {}_{N-1}\langle Q-1, S, r||V^{1/2}_{1/2}||Q, S\pm\tfrac{1}{2}, r'\rangle_{N-1}. \tag{A14}$$

The spectral function $B(\omega)$ obeys the sum rule

$$\int_{-\infty}^{\infty} \mathrm{d}\omega\ B(\omega) = \frac{1}{Z}\sum_{n} \mathrm{e}^{-\beta E_n}\langle n|f^{\dagger}_{\uparrow}f_{\uparrow}|n\rangle \equiv \langle f^{\dagger}_{\uparrow}f_{\uparrow}\rangle \tag{A15}$$

which can be easily derived by integrating equation (A1) over ω. In the particle–hole-symmetric case this gives

$$\int_{-\infty}^{\infty} \mathrm{d}\omega\ B(\omega) = \frac{1}{2} \tag{A16}$$

where we also find the following relation between $B(\omega)$ and $A(\omega)$:

$$B(\omega) + B(-\omega) = A(\omega). \tag{A17}$$

This can be directly obtained from equation (6).

References

[1] Anderson P W 1961 *Phys. Rev.* **124** 41
[2] Hewson A C 1993 *The Kondo Problem to Heavy Fermions* (Cambridge: Cambridge University Press)
[3] Tsvelik A M and Wiegmann P B 1983 *Adv. Phys.* **32** 453
Schlottmann P 1989 *Phys. Rep.* **181** 1
[4] Fye R M and Hirsch J E 1988 *Phys. Rev.* B **38** 433
[5] Keiter H and Kimball J C 1970 *Phys. Rev. Lett.* **25** 672
Pruschke Th and Grewe N 1990 *Z. Phys.* B **74** 439
[6] Yosida K and Yamada K 1970 *Prog. Theor. Phys. Suppl.* **46** 224
Horvatić B and Zlatić V 1985 *Solid State Commun.* **54** 957
[7] Wilson K G 1975 *Rev. Mod. Phys.* **47** 773
[8] Krishna-murthy H R, Wilkins J W and Wilson K G 1980 *Phys. Rev.* B **21** 1003
Krishna-murthy H R, Wilkins J W and Wilson K G 1980 *Phys. Rev.* B **21** 1044
[9] Sakai O, Shimizu Y and Kasuya T 1989 *J. Phys. Soc. Japan* **58** 3666
[10] Costi T A, Hewson A C and Zlatić V 1994 *J. Phys.: Condens. Matter* **6** 2519
[11] Metzner W and Vollhardt D 1989 *Phys. Rev. Lett.* **62** 324
[12] Mielsch C and Brandt U 1989 *Z. Phys.* B **75** 365
Janiś V 1991 *Z. Phys.* B **83** 227
Georges A and Kotliar G 1992 *Phys. Rev.* B **45** 6479
Jarrell M 1992 *Phys. Rev. Lett.* **69** 168
[13] Georges A, Kotliar G, Krauth W and Rozenberg M J 1996 *Rev. Mod. Phys.* **68** 13
[14] Sakai O and Kuramoto Y 1994 *Solid State Commun.* **89** 307
Shimizu Y and Sakai O 1995 *Computational Physics as a New Frontier in Condensed Matter Research* ed H Takayama *et al* (Tokyo: The Physical Society of Japan) p 42
[15] Bulla R, Pruschke Th and Hewson A C 1998 to be published
[16] Bulla R, Pruschke Th and Hewson A C 1997 *J. Phys.: Condens. Matter* **9** 10 463
[17] Hubbard J 1963 *Proc. R. Soc.* A **276** 238
Kanamori J 1963 *Prog. Theor. Phys.* **30** 257
Gutzwiller M C 1963 *Phys. Rev. Lett.* **10** 159
[18] Freericks J K and Jarrell M 1995 *Phys. Rev. Lett.* **74** 186
[19] Vollhardt D, Blümer N, Held K, Kollar M, Schlipf J and Ulmke M 1997 *Z. Phys.* B **103** 283
[20] Obermeier Th, Pruschke Th and Keller J 1997 *Phys. Rev.* B **56** 8479